ACS APPLIED MATERIALS & INTERFACES

Research Article

www.acsami.org

High-Performance Adhesives Resulting from Spontaneous Formation of Nanogels within Miniemulsion Particles

Vesna Daniloska,[†] Paula Carretero,[†] Radmila Tomovska,[†,‡] Maria Paulis,[†] and José M. Asua*[,†]

[†]POLYMAT and Departamento de Química Aplicada, Facultad de Ciencias Químicas, University of the Basque Country UPV/EHU, Joxe Mari Korta zentroa, Tolosa Hiribidea 72, Donostia-San Sebastián 20018, Spain

[‡]IKERBASQUE, Basque Foundation for Science, 48011 Bilbao, Spain

Supporting Information

ABSTRACT: Molecular structure plays a crucial role in determining the final properties of pressure-sensitive adhesives. Here, we demonstrate that the molecular structure of polyurethane/(meth)acrylic hybrids synthesized by miniemulsion photopolymerization changes during storage of the dispersion at room temperature because of the spontaneous formation of nanogels by the assembly of polymer chains within the polymer particles. Analysis of the nanogel structure by asymmetric-flow field-flow fractionation allows identification of the molecular structure that provides the unusual combination of high tack adhesion and excellent shear resistance at high temperature [maximum value of the shear-adhesion failure temperature (SAFT) test, >210 °C].

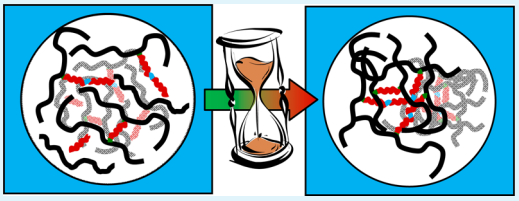

KEYWORDS: *nanogel, miniemulsion, AsFlFFF, PU/acrylic hybrids, pressure-sensitive adhesives*

1. INTRODUCTION

Miniemulsion polymerization[1−8] is the perfect technique to synthesize complex materials that cannot be produced otherwise such as adhesives,[9,10] antireflection,[11] anticorrosive[12] and UV-resistant coatings;[13] textile pigments,[14] gene and drug-delivery vectors,[15,16] polyolefin dispersions,[17] materials for tissue engineering,[18] and self-healing agents.[19] For applications in soft adhesives, miniemulsion polymerization allows the synthesis of polymer−polymer hybrids that combine the desired properties of each component. Thus, polyurethanes have been incorporated into acrylic polymers[10,20−22] in an attempt to increase the shear strength, which is usually low in waterborne pressure-sensitive adhesives (PSAs),[23,24] particularly at high temperatures.[25] However, the results available show that an increase in the shear strength is accompanied by a decrease in the tack adhesion.[10,20,26]

The properties of these materials are determined by polymer architecture, and one wonders if there is a polymer microstructure that provides at the same time high tack adhesion and high shear resistance at high temperature. However, attempts to link adhesion properties to the polymer microstructure[10,20,26,27] have been hindered by the fact that the characterization of these complex polymers is often limited to determination of the macroscopic gel content (fraction of the polymer film that is not soluble in a good solvent determined by Soxhlet extraction), the swelling capability of the gel, and the molecular weight distribution (MWD) of the soluble fraction extracted in the Soxhlet. Mathematical modeling[28−35] shed some light on the microstructure of the polymer, predicting that several nanogels (chemically or physically cross-linked nanosized networks), can coexist in the same particle. These models are difficult to validate because of the lack of experimental evidence about the polymer microstructure.

Asymetric-flow field-flow fractionation (AsFlFFF) allows fractionation of very large macromolecules and even particles of 400 nm.[36−39] This encompasses the expected size range of the nanogels (which should be smaller than the size of the miniemulsion particle, which in most cases is lower than 300 nm) and hence opens the possibility to directly analyze the nanogels.

In this work, AsFlFFF has been used to examine the evolution of the structure of nanogels coexisting in hybrid polyurethane/acrylic polymer particles that were synthesized by miniemulsion photopolymerization carried out in a tubular reactor. It is shown that, after leaving the reactor, the nanogels undergo an assembly process within the polymer particles over a period of several months. In the first few days, the assembly involves the formation of chemical (urea) bonds due to the reaction of the unreacted isocyanate groups with water. Later, assembly occurs by reversible interactions, presumably hydrogen bonding and perhaps entanglements resulting from polymer diffusion. It is also shown that the MWD of the polymer chains at the exit of the reactor and the assembly process determined the adhesion properties, showing for the first time that intraparticle interactions play a decisive role in the performance of these materials. This complements the classical view of the waterborne systems, where the focus has been on the importance of the particle−particle connectivity.[40−47] It is shown that the high contents of nanogels of

Received: December 13, 2013
Accepted: January 31, 2014
Published: January 31, 2014

 © 2014 American Chemical Society

relatively compact microstructure led to PSAs having an optimum combination of high tack adhesion and high shear resistance at high temperature.

2. EXPERIMENTAL SECTION

2.1. Materials. Technical-grade monomers, 2-ethylhexyl acrylate (2EHA; Quimidroga), methyl methacrylate (MMA; Quimidroga), methacrylic acid (MAA; Aldrich), and 2-hydroxyethyl methacrylate (HEMA; Fluka), were used as received. *N*-Octadecyl acrylate (SA; Aldrich) was used as a reactive costabilizer in order to prevent Ostwald ripening.[48,49] An aliphatic isocyanate-terminated polyurethane (PU) prepolymer, Incorez 701 (Incorez Ltd.) specially designed for adhesive applications, was used without further purification. The equivalent weight of the prepolymer is 1050 g/equiv. Dibutyltin dilaurate (DBTDL; Aldrich) was used as the catalyst for polyaddition reactions. Dowfax 2A1 (alkyl diphenyloxide disulfonate; Dow Chemicals) was used as the surfactant to prepare the miniemulsions, and sodium dodecyl sulfate (SDS; Aldrich) was added after miniemulsification to improve the miniemulsion stability. Both were used as received. The nonbleaching oil-soluble photoinitiator 1-hydroxycyclohexyl phenyl ketone (HCPK; Aldrich) was used as received. Sodium bicarbonate ($NaHCO_3$; Aldrich) was used as a buffer. Diethylamine (DEA; Aldrich), bromophenol indicator (Aldrich), hydrochloric acid (HCl; Aldrich), and sodium hydroxide (Aldrich) were used for the titrations of the free isocyanate (NCO) groups. Gel-permeation-chromatography-grade tetrahydrofuran (THF; Scharlau), toluene (HPLC grade from Sigma-Aldrich), and methanol (Scharlau) were used as solvents. Oxygen-free-grade nitrogen was used for purging the feed. Double-deionized water was used throughout this study.

2.2. Synthesis of the PU/Acrylic Hybrid Latexes. 45 wt % solids content miniemulsions were prepared based on the formulation shown in Table 1. First, the organic phase was prepared by dissolving Incorez 701 in the monomer mixture (2EHA/SA/MMA/MAA/HEMA). The photoinitiator HCPK was also dissolved in the organic phase. Then, the organic phase was mixed with an aqueous solution of the surfactant (Dowfax 2A1) and $NaHCO_3$ under intensive magnetic stirring (15 min at 1000 rpm) to create an emulsion. The resulting coarse emulsion was sonicated for 15 min at 9 output control and 80% duty cycle with a Branson 450 (Danbury, CT). The temperature after sonication was around 68 °C. Finally, in order to improve the miniemulsion stability, SDS was added. After the addition, the miniemulsion was cooled to room temperature under agitation (approximately 2 h).

Table 1. 45 wt % Solids Content PU/(Meth)acrylic Miniemulsion Formulation (Reaction Temperature: 25 °C)

component	amount (g)	wt %
2EHA	196.43	91.5[a]
SA	12.5	5.8[a]
MMA	3.04	1.4[a]
MAA	2.03	0.9[a]
HEMA	1.01	0.4[a]
PU	22.5	10[b]
DBTDL	0.11	500 ppm[c]
HCPK	0.505	0.24[a]
double-deionized water	270.05	
Dowfax 2A1	9	2 (45 wt % active)[b]
$NaHCO_3$	0.46	0.02 M[d]
SDS	2.25	1[b,e]

[a]Weight based on the monomer weight. [b]Weight based on the organic weight. [c]ppm based on the organic phase. [d]Based on the water phase. [e]After miniemulsification addition.

The polymerizations were performed in a continuous tubular reactor composed of a 74 cm silicone tube (2 mm inner diameter) and seven quartz tubes connected with each other with six semicircular silicone bends (2 mm inner diameter). Each quartz tube had a length of 400 mm, an inner diameter of 1 mm, and an outer diameter of 3 mm. These two materials were used for the design of the reactor in order to avoid clogging of the reactor.[50] A UV chamber (model BS 03, Dr. Gröbel UV-Elektronik GmbH) equipped with 20 UV lamps giving UV light in the range from 315 to 400 nm with a maximum at 368 nm was used. The incident light irradiance (ILI) was measured using a radiometer UV sensor. A gear pump (model 305, Gilson) was used to feed the miniemulsion (that was kept under stirring at 450 rpm) to the reactor with a flow rate corresponding to a residence time of 10 min, which was enough to achieve almost complete conversion of the acrylic monomers at the reactor outlet. Prior to being fed to the reactor, the miniemulsion was purged with nitrogen for about 30 min. The latexes analyzed were obtained under steady-state conditions. The reaction temperature was measured at the inlet and outlet of the reactor, and it was found that it was 25 ± 1 °C in both places. This shows that the reactor made from narrow quartz tubes efficiently removed the heat of polymerization. Without UV irradiation, no polymerization of the (meth)acrylates took place even in the presence of the initiator. Moreover, direct irradiation of the monomer without the photoinitiator did not lead to formation of the polymer.

Two different latexes were prepared using the formulation given in Table 1. The difference between them was the ILI applied in their synthesis, which was 3.5 mW/cm^2 in the case of latex 1 (L1) and 2.5 mW/cm^2 in the case of latex 2 (L2). In this process, the hybrid PU/acrylic polymer is formed by free-radical polymerization of the (meth)acrylic monomers and addition polymerization of the isocyanate groups with the hydroxyl groups of HEMA and water present in the miniemulsion droplet/particle. The reason to include PU in the formulation is to improve the poor performance of the acrylic PSAs at high temperatures.[10,20,51]

2.3. Characterization. Dynamic light scattering (Zetasizer Nano Z, Malvern Instruments) was used to measure the miniemulsion droplet and latex particle *z*-average diameters. Samples were prepared by diluting one drop of latex or miniemulsion in deionized water. The reported diameters are the average of two measurements. The (meth)acrylic monomer conversion was determined gravimetrically at the reactor outlet. The amount of unreacted NCO in the organic phase, miniemulsion, and reactor outlet was measured by back-titration with HCl of excess DEA molecules nonreacted with free NCO.[52] Bromophenol blue was used as the indicator solution. A detailed description of this titration can be found in the Supporting Information (SI). The macroscopic gel content of dried samples was determined gravimetrically by Soxhlet extraction under THF reflux. Details of the method are given in the SI.

In this work, different techniques were used for determination of the MWD of the samples. Size-exclusion chromatography (SEC) was used for the PU prepolymers [with a refractive index (RI) detector] and the soluble fraction of the PU/acrylic hybrid [with multiangle light scattering (MALS) and RI detectors]. Further details are given in the SI. The whole MWD of the PU/acrylic hybrid polymer was determined by AsFlFFF (AF4, Wyatt Eclipse 3) using THF as the solvent and MALS and RI detectors. In this method, the separation is based on the interplay between the flows of the carrier and the Brownian motion of the macromolecules occurring in an open channel. The upper plate of the channel is impermeable, whereas the bottom plate is permeable. This allows creation of a flow along the channel and a cross-flow perpendicular to the channel. The equilibrium between the cross-flow and Brownian motion creates a concentration distribution of the macromolecules, with the larger ones being placed near to the bottom of the channel and the smaller ones closer to the center of the channel, where the velocity of the laminar flow along the channel is higher. Therefore, the small macromolecules elute before the larger ones. The big advantage of AsFlFFF is that very large macromolecules can be analyzed. Further experimental details of this technique can be found in the SI.

Adhesive Properties. The adhesive properties measured were the work of adhesion by probe-tack tests, peel strength, and cohesive strength by a shear-adhesion failure temperature (SAFT) test (see the SI for further experimental details). The films for measuring the

adhesive properties were prepared on electrostatic discharge-treated 29-μm-thick polypropylene foils for peel tests and 23-μm-thick Mylar polyester foils for SAFT measurements. A 120 μm wet film was placed over these supports and dried for 4 h at room temperature. The thicknesses of the final dry films were 50−55 μm.

3. RESULTS AND DISCUSSION

Table 2 presents the characteristics of the two latexes synthesized by miniemulsion polymerization using the formulation given in Table 1 under different incident light intensities, 3.5 mW/cm^2 (L1) and 2.5 mW/cm^2 (L2). These characteristics were measured just after the reaction.

Table 2. Characteristics of the Hybrid PU/Acrylic Latexes

latex	droplet size (nm)	particle size (nm)	(meth)acrylate conversion (wt %)	macroscopic gel fraction (wt %)	Sol $\overline{M}_w$ (g/mol)
L1	148	149	97	65	255900
L2	152	154	96	69	308600

It can be seen that the particle size and final conversion of the (meth)acrylates were very similar in both cases. On the other hand, both latexes showed a substantial macroscopic gel fraction, as measured by Soxhlet extraction (slightly higher for L2), and the sol molecular weight was higher for L2, which was produced with lower ILI. Lower ILI induced the formation of fewer radicals, leading to longer kinetic chain length of the (meth)acrylic chains. Furthermore, the longer the (meth)-acrylic chain, the higher the cross-linking probability because more HEMA monomer units are likely to be found incorporated in the main chain. These units are responsible of reacting with NCO groups from PU to form cross-links.

Figure 1 presents the MWD of latexes L1 and L2 measured by AsF1FFF just after the reaction. The MWDs of the sol fractions obtained from Soxhlet extraction measured by SEC-MALS are included for the sake of comparison. The AsF1FFF measurement corresponds to the whole polymer, whereas that of SEC-MALS is only the soluble fraction. For both L1 and L2, the MWD determined by AsF1FFF showed the presence of a fraction of high-molecular-weight polymer that was not observed by SEC-MALS, but this fraction was substantially lower than the macroscopic gel fractions given in Table 2.

One possible explanation for the high macroscopic gel contents given in Table 2 could be the sample preparation used in these measurements, which involved drying of the polymer dispersion at 60 °C for 24 h before Soxhlet extraction, while the sample analyzed by AsF1FFF was maintained at room temperature. In order to check whether this was the reason for the difference, the macroscopic gel content of L1 was measured again, drying the polymer at room temperature under vacuum before Soxhlet extraction. The macroscopic gel fraction measured under these conditions was only 10%. The most plausible reason for the effect of the drying temperature on the gel fraction was the reaction of the hydroxyl groups of the HEMA units of the acrylic polymer chains with the isocyanate groups that did not react during miniemulsion preparation and polymerization in the tubular reactor. In addition, chain extension of PU by urea groups formed upon reaction of the isocyanate groups with water cannot be discarded.

These reactions can also occur at room temperature, leading to changes in the microstructure of the polymer during storage. Figure 2 presents the evolution of the MWDs of L1 and L2 measured by AsF1FFF over several months. It can be seen that the MWDs shifted toward higher values for the whole period of time (up to 230 days). Figure 2 clearly shows that the MWD evolves from a broad but basically monomodal distribution to a bimodal distribution with a mode in the range of 10^5 g/mol and a mode composed by nanogels [M_w > (5−10) × 10^6 g/mol]. Table 3 presents the evolution during storage of the nanogel content calculated from the AsF1FFF chromatograms by considering nanogels the macromolecules with size greater than 5 × 10^6 g/mol. This value was chosen because it corresponds to the highest molecular weight observed for the MWD of the soluble fraction extracted from the Sohxlet. Furthermore, the average molecular weights of the polymer below and above such a limit are also displayed in Table 3.

The relative importance of the smaller molecular weight mode decreased over time, indicating a continuous incorporation of smaller chains to the nanogels. In addition, the size of the nanogels increased with time, showing an assembly of the nanogels. Although qualitatively, the evolution of the MWDs of L1 and L2 is similar, a comparison between them shows the effect of the initial MWD. It can be seen that, because of the higher initial molecular weights, the nanogels formed faster and grew to larger size for L2 (100 × 10^6 g/mol) than for L1 (49.1 × 10^6 g/mol).

It is interesting to compare the size of the nanogels with that of the polymer particles. For a density of 1.1 kg/L, the nanogels in L1 after 57 days (M_w = 21.1 × 10^6 g/mol) can be represented by spheres of about 40 nm diameter, namely, much

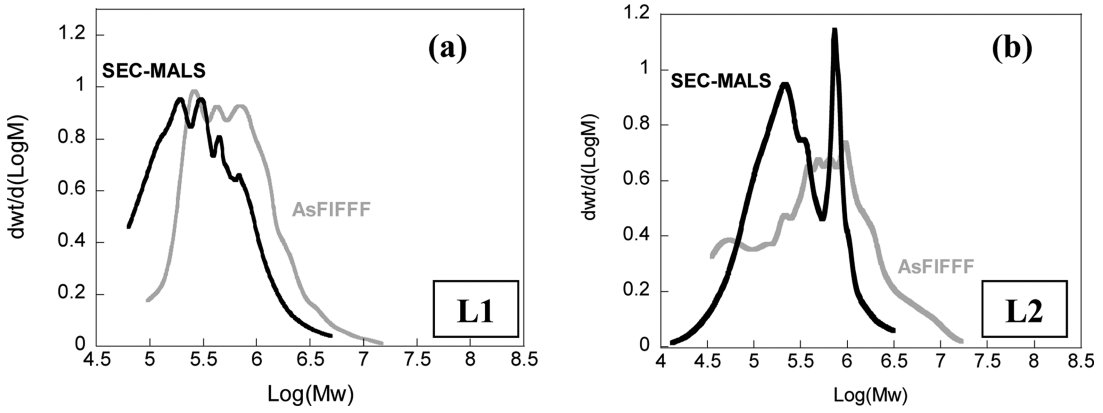

Figure 1. MWDs of L1 (a) and L2 (b) determined by AsF1FFF for the whole latex (in gray) and by SEC-MALS for the sol fraction obtained from Soxhlet extraction (in black) just after reaction.

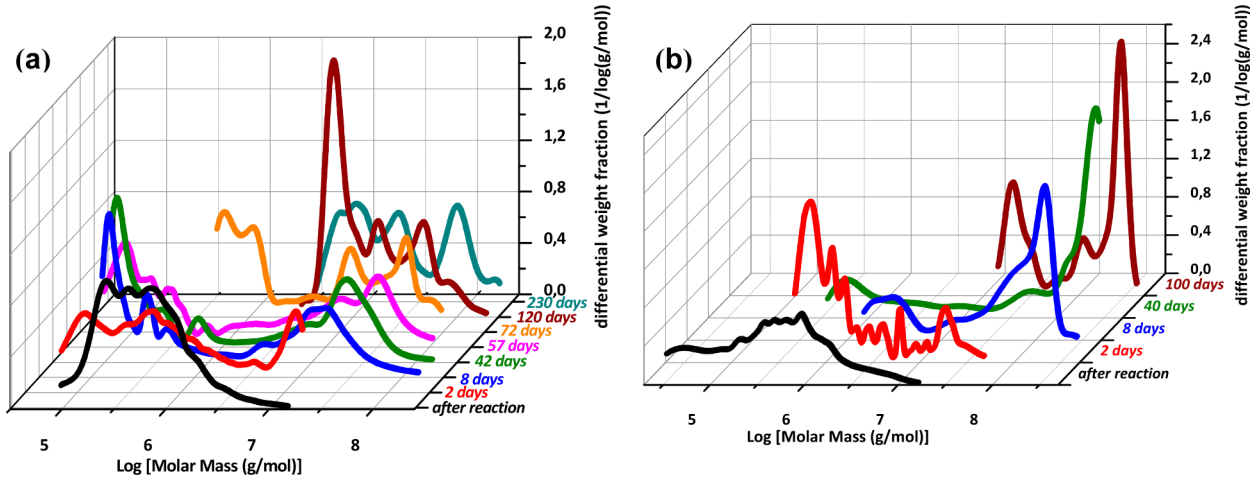

Figure 2. Evolution of the whole MWDs of L1 (a) and L2 (b) with time at room temperature using AsF1FFF.

Table 3. Evolution of the Microstructures of L1 and L2 Latexes with Time As Measured by AsF1FFF

latex	storage time at room temperature (days)	% nanogel	M_w lower mode (g/mol)	M_w larger mode (g/mol)
L1	0	2	0.55×10^6	7.5×10^6
	2	18	0.46×10^6	9.86×10^6
	8	40	0.44×10^6	17.5×10^6
	42	42	0.40×10^6	19.8×10^6
	57	40	0.32×10^6	21.1×10^6
	72	52	1.38×10^6	22.2×10^6
	120	95		15.9×10^6
	230	100		49.1×10^6
L2	0	8	0.37×10^6	5.7×10^6
	2	28	0.95×10^6	11.7×10^6
	8	87	2.24×10^6	49.3×10^6
	40	76	0.91×10^6	100.2×10^6
	100	100		101.4×10^6

Table 4. Reacted Isocyanate Groups Percentage along the Process

step	experimental X_{NCO} (%) by titration
organic phase, *after mixing*	6.6
miniemulsion, *after sonication*	49.8
miniemulsion, *after 5 h of mixing (entrance of the reactor)*	68.7
latex, *exit of the reactor*	68.7
latex, *8 days after reaction*	100

smaller than the size of the polymer particles (≈150 nm). This means that, even for a relatively low nanogel fraction, one particle may contain several nanogels (e.g., for a nanogel fraction of 40%, the particle would contain 21 of these nanogels). After 230 days, the nanogel size of L1 would be 52 nm, and still a large number of nanogels would coexist (24) within the particle. The nanogels formed in L2 after 100 days (M_w = 101 × 10^6 g/mol) can be represented by spheres of about 70 nm; namely, one particle can contain a few of these large nanogels, although they can coexist with other smaller ones.

In order to shed light on the reasons for the formation and evolution of the nanogels, the isocyanate groups were titrated during miniemulsion preparation, at the entrance and exit of the tubular reactor and during the storage time (Table 4).

It can be seen that about 7% of the NCO groups reacted during formation of the organic phase, presumably with HEMA, although some reaction with traces of water cannot be discounted. The conversion of NCO increased to almost 50% during miniemulsification because of the presence of water and the increase in temperature caused by miniemulsification. NCO conversion further increased, maintaining miniemulsion at rest for 5 h, but no reaction of the NCO groups occurred in the tubular reactor for the 10 min of residence time used. During storage, the reaction of NCO with water continued, and after 8 days, no trace of NCO groups was detectable.

This means that the increase in the fraction and size of the nanogels occurring during the first 8 days of storage may be caused by urea links formed by the reaction of NCO with water. However, Figure 2 shows that the fraction of nanogels and their size continued to increase during the whole period studied (up to 230 days). In the absence of reactive groups, the evolution of the nanogels could be due to the formation of hydrogen bonds and/or entanglements. If this was the case, "nanogelification" would be reversible.

In order to check this point, the aged polymer dispersions (120 days for L1 and 100 days for L2) were diluted in water and then slowly added to THF up to a concentration of 7 mg of polymer/mL of THF. The objective of this procedure was to minimize particle−particle coagulation during transfer of the particles from the aqueous system to THF. In THF, the low-molecular-weight polymer will readily become dissolved and the physically entangled nanogels (if any) will disentangle with time. Therefore, the system was kept at 70 °C in closed vessels and the evolution of the MWD measured by AsF1FFF. Figure 3 presents these results. The MWDs of the aged samples (120 days for L1 and 100 days for L2) are also included. In addition, the MWDs after 8 days of aging (moment in which no NCO could be detected) are included as a reference. It can be seen that the relative fraction and molecular weights of the nanogels decreased with the time spent by the samples in THF at 70 °C.

In order to attribute this effect to disentanglements, the stability of the urea and urethane bonds under the conditions used in the test (70 °C in THF) should be assessed. For that aim, diisocyanate-terminated PU was dissolved in THF containing water in a ratio H_2O/NCO = 3, and the polyaddition polymerization was performed until all NCO groups reacted. This resulted in an increase of the molecular weight of PU. Then, the system was heated to 70 °C, and the

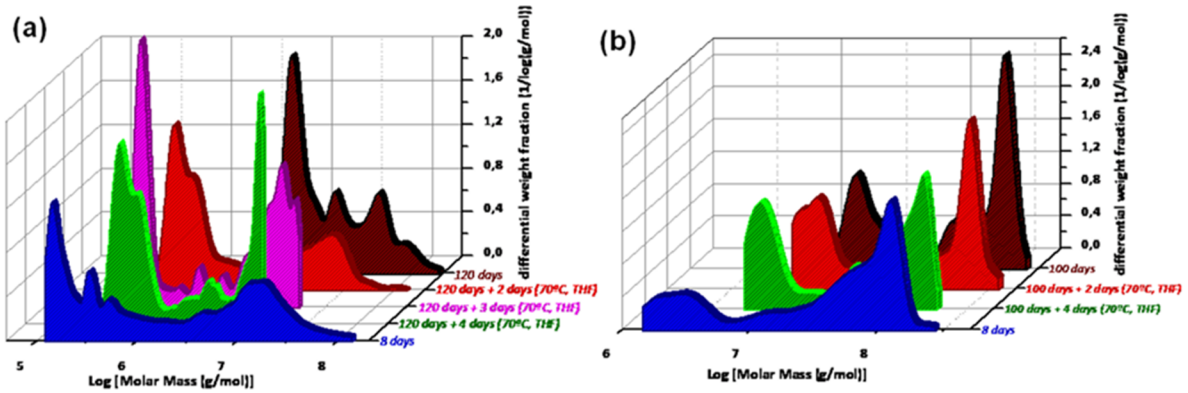

Figure 3. Evolution of the complete MWDs of L1 (a) and L2 (b) in the disentanglement experiments carried out in THF at 70 °C. The MWDs of the samples aged at 8 days and maximum aging time (120 days for L1 and 100 days for L2) are included as reference.

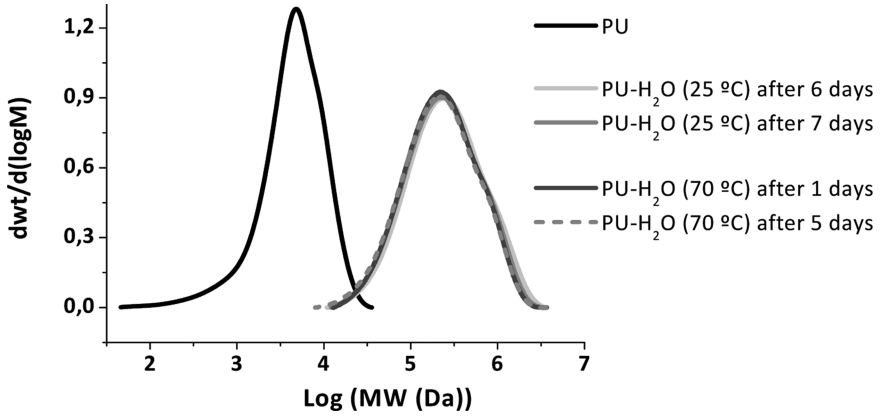

Figure 4. Evolution of the MWD during addition polymerization of PU and water at room temperature in THF and during subsequent heating at 70 °C under stirring.

evolution of the MWD was measured. Figure 4 shows that no variation of the MWD was observed for 5 days, meaning that the urea and urethane bonds were stable for this period of time. Therefore, the disentanglements observed in Figure 3 in 4 days at 70 °C in THF were due to reversible hydrogen bonding and/or other physical linkages.

Scheme 1 summarizes formation of the polymer microstructure in this system. During the preparation of the miniemulsion, isocyanate-terminated PU reacts with HEMA (yielding double-bond-terminated PUs) and with water (extending the PU chains by means of urea groups). In the reactor, the (meth)acrylic chains are formed. The (meth)acrylic chains contain PU chains linked through urethane groups to the HEMA units. Some cross-linking is expected from the PU chains containing two double bonds at the entrance of the reactor. Because the residence time in the reactor is very short (10 min) and polymerization is carried out at 25 °C, no polyaddition occurs in the reactor, and hence at the exit of the reactor, there is still a certain amount of isocyanate groups. The MWDs measured at the exit of the reactor show the presence of high-molecular-weight polymer (Figure 2), which may be considered as nanogel precursors. During storage, the remaining isocyanate groups react with the water dissolved in the polymer particles and further cross-linking occurs through the formation of urea groups, increasing the size and amount of the nanogels. After 8 days of storage, all isocyanate groups are reacted and no further polyaddition occurs. From this moment on, hydrogen bonding and other physical interactions are responsible for the formation of nanogels. These reversible mechanisms caused the substantial increase of both the relative amount and molecular weight of the nanogels.

The effect of the changes in the polymer microstructure occurring during storage on the adhesive properties was studied. The work of adhesion was measured in the probe-tack experiments presented in Figure 5. In these experiments, first the probe comes into contact with the adhesive film, and afterward, when the probe is elevated from the adhesive, a negative pressure is created, which induces the formation of cavities. The number of cavities reaches a maximum at maximum stress. Later on, the stress falls to a plateau because of propagation of the cavities laterally and vertically as the walls between the cavities are drawn into fibrils.[53−55] The force that is needed to draw the fibrils determines the plateau stress at higher strains. Finally, the stress drops to zero when the fibrils break or detach from the probe at maximum strain. The area under the stress−strain curve is the work of adhesion. The values of the work of adhesion as well as those of the peel strength and SAFT are presented in Tables 5 and 6 for L1 and L2, respectively. These tables show that the adhesion properties change during storage of the latexes because of the assembly of nanogels within the polymer particles. This sheds new light on the effect of storage on the adhesion properties because in the previous works attention was focused on the effect of the storage time of films on the adhesion properties, which was linked to interparticle interactions during film formation.[40−47]

dx.doi.org/10.1021/am405752k | ACS Appl. Mater. Interfaces 2014, 6, 3559−3567

Scheme 1. Proposed Evolution of the Microstructure during and after Reaction[a]

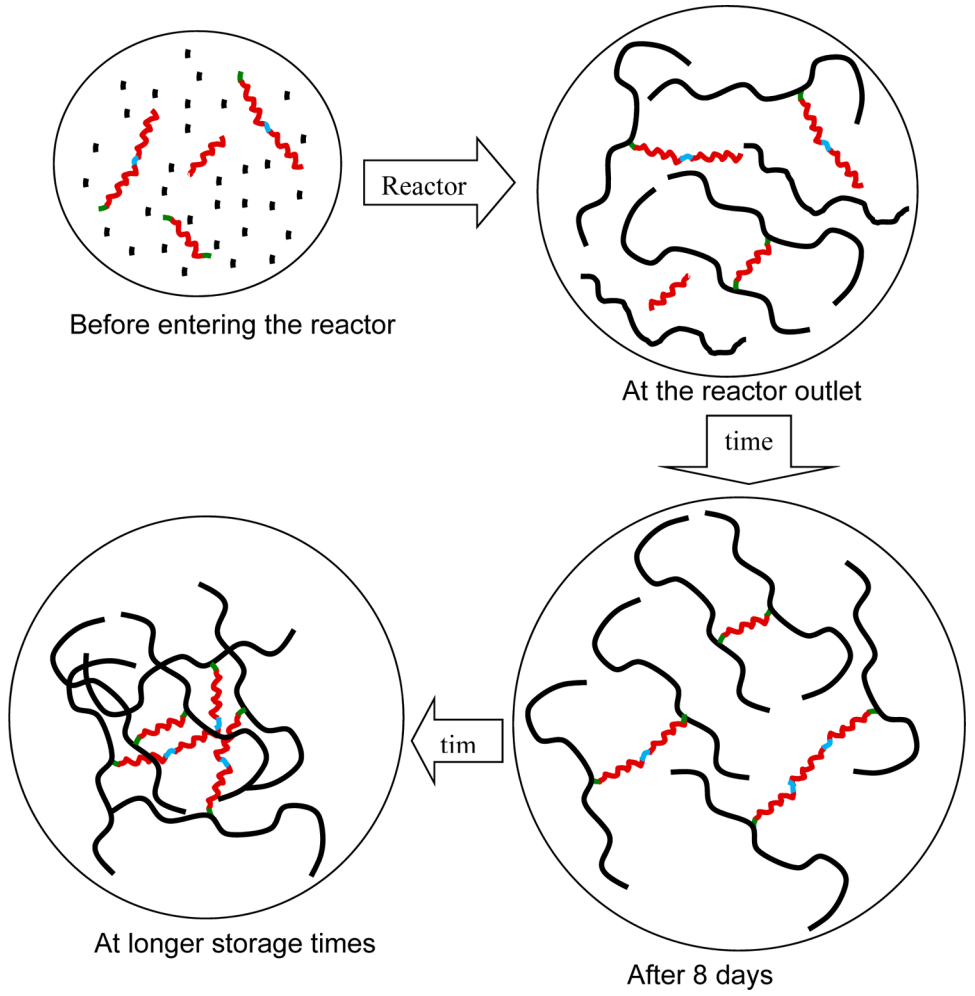

[a]PU: red chains. HEMA: green chains. Acrylic monomers: black chains. Urea bonds: blue linkages.

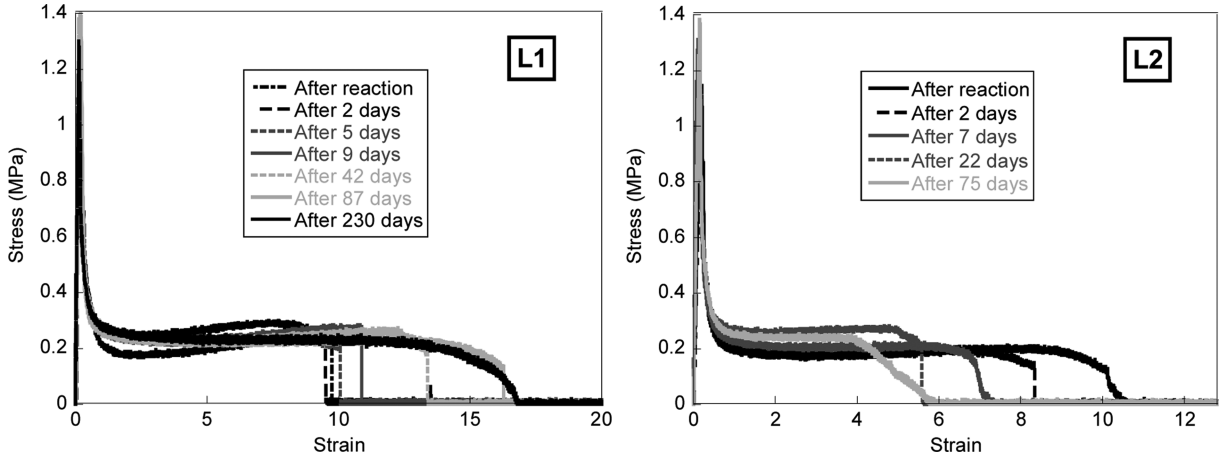

Figure 5. Probe-tack stress–strain curves of L1 and L2 films at different storage times.

Figure 5 shows that, in the case of L1, the maximum strain increased during storage up to 87 days, which affected the work of adhesion (Table 5). The maximum strain occurs when either the fibrils fracture (cohesive failure) or the adhesive detaches from the substrate (adhesive failure). Unfortunately, the presence of residual polymer in the probe, which is a fingerprint of cohesive failure, was not checked. The abrupt fall of the stress at maximum strain in the probe-tack experiments suggests adhesive failure. Adhesive failure occurs when the energy for crack propagation is lower than the energy needed to elongate the fibrils. The ratio of these energies is given by[56]

$$H/G_0 \frac{\tan \delta}{E}$$

dx.doi.org/10.1021/am405752k | ACS Appl. Mater. Interfaces 2014, 6, 3559–3567

Table 5. Adhesive Properties of L1 Stored at Room Temperature

storage time at room temperature (days)	work of adhesion (J/m^2)	peel (N/25 mm)	SAFT (°C)
0	128.3	5.1 ± 0.3	>210
2	139.2	6.2 ± 0.5	>210
5	138.6	6.3 ± 0.2	>210
9	151.2	6.3 ± 0.2	>210
42	173.2	6.5 ± 0.5	>210
87	220.4	7.5 ± 0.1	>210
230	211.0	6.0 ± 0.4	>210

Table 6. Adhesive Properties of L2 Stored at Room Temperature

storage time at room temperature (days)	work of adhesion (J/m^2)	peel (N/25 mm)	SAFT (°C)
0	114.89	6.0 ± 0.3	>210
2	92.56	5.6 ± 0.1	>210
7	90.25	5.4 ± 0.2	>210
22	87.34	5.0 ± 0.1	>210
75	76.34	4.2 ± 0.2	>210

where G_0 is the resistance to crack propagation at vanishingly low crack velocity and E Young's modulus. Large values of H lead to cohesive failure, whereas small values give adhesive failure. The ratio tan δ/E usually increases with the molecular weight; therefore, the likelihood of adhesive failure is expected to increase with the molecular weight. This would result in a decrease of the maximum strain with the molecular weight, which is the opposite of what is observed in Figure 5, casting doubts to the adhesive failure. Another possibility is that at low and intermediate gel contents cohesive failure occurred. The increase of the nanogel content made the fibrils more cohesive, and the fracture was delayed to larger strains. Above 87 days, the increase of the molecular weight of the nanogels caused by the storage time had almost no effect on the maximum strain, although a small decrease of the work of adhesion was observed.

For L2, the work of adhesion decreased with the nanogel content (as the storage time increased). This means that, even for moderate values of the nanogel content, the polymer was too cohesive. A comparison with the results obtained with L1 shows that, for the same values of nanogel fraction, L2 showed higher cohesiveness. The reason may be the microstructure of the nanogel network. Figure 6 shows that, for a given molecular weight, the radius of gyration of L2 was much larger than that for L1. This means that, for a given molecular weight, the nanogels of L1 were more compact than those of L2. Therefore, for a given nanogel content, the effective volume occupied by the nanogels was higher for L2 than for L1, and hence the nanogels had a higher interconnectivity, which was the reason for the higher cohesiveness and lower work of adhesion. Figure 6 also shows that for low molecular weights ($M_w < 10^6$ g/mol) the radius of gyration scales with the molecular weight to a power of 0.6, suggesting that these chains were relatively linear. For higher molecular weights, a much lower power was found, indicating that the macromolecules were highly branched.

Tables 5 and 6 show that the nanogel content affected the peel strength in the same way as it did for the work of adhesion. The decrease observed for L1 230 days after the reaction, which was accompanied by a small decrease in the work of adhesion,

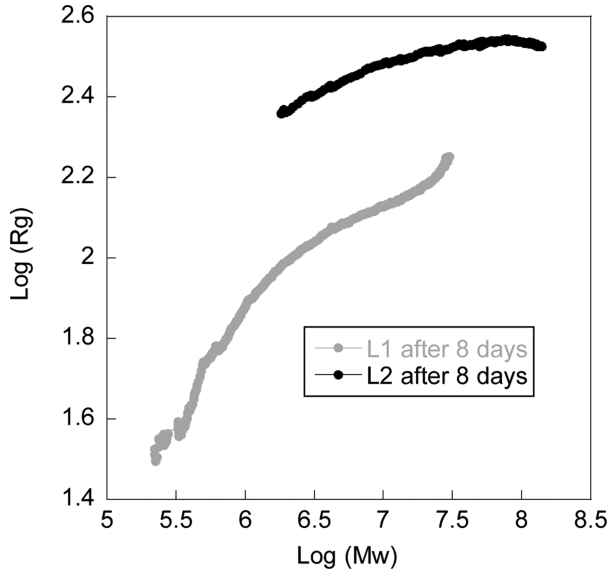

Figure 6. Variation of the radius of gyration (R_g, nm) versus M_w of L1 and L2 measured after 8 days (quantified from the AsFlFFF curves).

indicates that the polymer became too stiff. This may be related to the observed effects of the macroscopic gel on the tack and work of adhesion.[57−60] Tables 5 and 6 also show that all samples reached the maximum value in the SAFT test (>210 °C), showing excellent cohesion at high temperatures. It is somehow surprising that even the sample directly obtained from the reactor yielded such a high value of SAFT because it contained almost no nanogel and the molecular weights were not high (Table 3 and Figure 2). The reason may be that, because of the temperature increase implemented during the SAFT test, the remaining NCO groups reacted, causing cross-linking among the (meth)acrylate chains.

4. CONCLUSIONS

In this work, it is shown that PU/(meth)acrylic PSAs synthesized by miniemulsion photopolymerization undergo spontaneous formation of nanogels within the miniemulsion particles during storage at room temperature. The evolution of the nanogel structure was studied by means of asymmetric-flow field-flow fractionation. In the first few days, nanogels were formed by the assembly of polymer chains by the formation of urea groups resulting from the reaction of isocyanate groups and water absorbed in the polymer particles. After about 8 days of storage, all isocyanate groups were reacted and the assembly of nanogels occurred by reversible interactions, presumably hydrogen bonding and perhaps entanglements resulting from polymer diffusion. The assembly of nanogels continued for a period of several months, resulting in a strong change of the polymer microstructure. Nanogels formed by the assembly of shorter (meth)acrylic chains were more compact than those formed from longer (meth)acrylic chains. The nanogels with open structure had a high interconnectivity even for moderate values of the nanogel content, which made them too stiff, leading to lower and continuously decreasing values of the work of adhesion with the nanogel content. For the more compact nanogels, at low and intermediate nanogel contents, an increase of the work of adhesion and peel strength was observed. High contents of nanogels of relatively compact structure formed by shorter (meth)acrylate chains led to PSAs having the optimum combination of high tack adhesion and excellent shear

resistance at high temperature (maximum value of the SAFT test, >210 °C).

■ ASSOCIATED CONTENT

Supporting Information

Detailed experimental procedures of the characterization techniques used in this work such as quantification of the unreacted NCO groups, measurement of the macroscopic gel content, measurements of the MWD by different techniques (SEC-RI, SEC-MALS-RI, and AsFlFFF-MALS-RI), and quantification of the adhesive properties. This material is available free of charge via the Internet at http://pubs.acs.org.

■ AUTHOR INFORMATION

Corresponding Author

*E-mail: jm.asua@ehu.es.

Notes

The authors declare no competing financial interest.

■ ACKNOWLEDGMENTS

Diputación Foral de Gipuzkoa, University of Basque Country (UFI 11/56), Basque Government (Grant GVIT373-10 and Etortek Nanoiker IE11-304), and Ministerio de Economía y Competitividad (Grant CTQ2011-25572) are grateful acknowledged for their financial support.

■ REFERENCES

(1) Ugelstad, J.; El-Aasser, M. S.; Vanderhoff, J. W. Emulsion Polymerization: Initiation of Polymerization in Monomer Droplets. *J. Polym. Sci., Polym. Lett. Ed.* **1973**, *11*, 503−513.

(2) El-Aasser, M. S.; Miller, C. M. In *Polymeric Dispersion: Principles and Applications*; Asua, J. M., Ed.; Kluwer: Dordrecht, The Netherlands, 1997.

(3) Blythe, P. J.; Sudol, E. D.; El-Aasser, M. S. Recent Advances in Miniemulsion Polymerization. *Macromol. Symp.* **2000**, *150*, 179−186.

(4) Capek, I.; Chern, C. S. Radical Polymerization in Direct Mini-Emulsion Systems. *Adv. Polym. Sci.* **2001**, *155*, 101−165.

(5) Antonietti, M.; Landfester, K. Polyreactions in Miniemulsions. *Prog. Polym. Sci.* **2002**, *27*, 689−757.

(6) Asua, J. M. Miniemulsion Polymerization. *Prog. Polym. Sci.* **2002**, *27*, 1283−1346.

(7) Schork, F. J.; Luo, Y.; Smulders, W.; Russum, J. P.; Butte, A.; Fontenot, K. Miniemulsion Polymerization. *Adv. Polym. Chem.* **2005**, *175*, 129−255.

(8) Landfester, K. Miniemulsion Polymerization and the Structure of Polymer and Hybrid Nanoparticles. *Angew. Chem., Int. Ed.* **2009**, *48*, 4488−4507.

(9) Agirre, A.; de las Heras-Alarcon, C.; Wang, T.; Keddie, J. L.; Asua, J. M. Waterborne, Semicrystalline, Pressure-Sensitive Adhesives with Temperature-Responsiveness and Optimum Properties. *ACS Appl. Mater. Interfaces* **2010**, *2*, 443−451.

(10) Lopez, A.; Degrandi-Contraires, E.; Canetta, E.; Creton, C.; Keddie, J. L.; Asua, J. M. Waterborne Polyurethane−Acrylic Hybrid Nanoparticles by Miniemulsion Polymerization: Applications in Pressure-Sensitive Adhesives. *Langmuir* **2011**, *27*, 3878−3888.

(11) Sun, Z.; Luo, Y. Fabrication of Non-Collapsed Hollow Polymeric Nanoparticles with Shell Thickness in the Order of Ten Nanometres and Anti-Reflection Coatings. *Soft Matter* **2011**, *7*, 871−875.

(12) Bhadra, S.; Singha, N. K.; Khastgir, D. Polyaniline Based Anticorrosive and Anti-Molding Coating. *J. Chem. Eng. Mater. Sci.* **2011**, *2*, 1−11.

(13) Aguirre, M.; Paulis, M.; Leiza, J. R. UV Screening Clear Coats Based on Encapsulated CeO_2 Hybrid Latexes. *J. Mater. Chem. A* **2013**, *1*, 3155−3162.

(14) Abdou, L. A. W.; El-Molla, M. M.; Hakeim, O. A.; El-Gammal, M. S.; Shamey, R. Synthesis of Nanoscale Binders through Mini Emulsion Polymerization for Textile Pigment Applications. *Ind. Eng. Chem. Res.* **2013**, *52*, 2195−2200.

(15) Lorenz, S.; Hauser, C. P.; Autenrieth, B.; Weiss, C. K.; Landfester, K.; Mailander, V. The Softer and More Hydrophobic the Better: Influence of the Side Chain of Polymethacrylate Nanoparticles for Cellular Uptake. *Macromol. Biosci.* **2010**, *10*, 1034−1042.

(16) Tautzenberger, A.; Lorenz, S.; Kreja, L.; Zeller, A.; Musyanovych, A.; Schrezenmeier, H.; Landfester, K.; Mailander, V.; Ignatius, A. Effect of Functionalised Fluorescence-Labelled Nanoparticles on Mesenchymal Stem Cell Differentiation. *Biomaterials* **2010**, *31*, 2064−2071.

(17) Sauca, S. N.; Asua, J. M. Catalytic Polymerization of Ethylene in Aqueous Media. *Chem. Eng. J.* **2011**, *168*, 1319−1330.

(18) Bencherif, S. A.; Washburn, N. R.; Matyjaszewski, K. Synthesis by AGET ATRP of Degradable Nanogel Precursors for In Situ Formation of Nanostructured Hyaluronic Acid Hydrogel. *Biomacromolecules* **2009**, *10*, 2499−2507.

(19) Fickert, J.; Makowski, M.; Kappl, M.; Landfester, K.; Crespy, D. Efficient Encapsulation of Self-Healing Agents in Polymer Nanocontainers Functionalized by Orthogonal Reactions. *Macromolecules* **2012**, *45*, 6324−6332.

(20) Lopez, A.; Degrandi, E.; Canetta, E.; Keddie, J. L.; Creton, C.; Asua, J. M. Simultaneous Free Radical and Addition Miniemulsion Polymerization: Effect of the Diol on the Microstructure of Polyurethane−Acrylic Pressure-Sensitive Adhesives. *Polymer* **2011**, *52*, 3021−3030.

(21) Udagama, R.; Degrandi-Contraires, E.; Creton, C.; Graillat, C.; McKenna, T. F. L.; Bourgeat-Lami, E. Synthesis of Acrylic−Polyurethane Hybrid Latexes by Miniemulsion Polymerization and Their Pressure-Sensitive Adhesive Applications. *Macromolecules* **2011**, *44*, 2632−2642.

(22) Degrandi-Contraires, E.; Udagama, R.; Bourgeat-Lami, E.; McKenna, T.; Ouzineb, K.; Creton, C. Mechanical Properties of Adhesive Films Obtained from PU−Acrylic Hybrid Particles. *Macromolecules* **2011**, *44*, 2643−2652.

(23) Tobing, S. D.; Klein, A. Molecular Parameters and their Relation to the Adhesive Performance of Acrylic Pressure-Sensitive Adhesives. *J. Appl. Polym. Sci.* **2001**, *79*, 2230−2244.

(24) Jovanović, R.; Dubé, M. A. Emulsion-Based Pressure-Sensitive Adhesives: A Review. *J. Macromol. Sci., Polym. Rev.* **2004**, *44*, 1−51.

(25) Satas, D. Acrylic Adhesives. In *Handbook of Pressure Sensitive Adhesive Technology*; Satas, D., Eds.; Van Nostrand Reinhold: New York, 1989.

(26) Degrandi-Contraires, E.; Lopez, A.; Reyes, Y.; Asua, J. M.; Creton, C. High-Shear-Strength Waterborne Polyurethane/Acrylic Soft Adhesives. *Macromol. Mater. Eng.* **2013**, *298*, 612−623.

(27) Creton, C.; Kramer, E. J.; Brown, H. R.; Hui, C. Y. Adhesion and Fracture of Interfaces Between Immiscible Polymers: From the Molecular to the Continuum Scale. *Adv. Polym. Sci.* **2002**, *156*, 53−136.

(28) Arzamendi, G.; Asua, J. M. Modeling Gelation and Sol Molecular Weight Distribution in Emulsion Polymerization. *Macromolecules* **1995**, *28*, 7479−7490.

(29) Tobita, H.; Kumagai, M.; Aoyagi, N. Microgel Formation in Emulsion Polymerization. *Polymer* **2000**, *41*, 481−487.

(30) Butte, A.; Storti, G.; Morbidelli, M. Microgel Formation in Emulsion Polymerization. *Macromol. Theory Simul.* **2007**, *16*, 441−457.

(31) Reyes, Y.; Lopez, A.; Asua, J. M. Modeling the Microstructure of Acrylic−Polyurethane Hybrid Polymers Synthesized by Miniemulsion Polymerization. *Macromol. React. Eng.* **2011**, *5*, 352−360.

(32) Hamzehlou, S.; Reyes, Y.; Leiza, J. R. Detailed Microstructure Investigation of Acrylate/Methacrylate Functional Copolymers by Kinetic Monte Carlo Simulation. *Macromol. React. Eng.* **2012**, *6*, 319−329.

(33) Kryven, I.; Berkenbos, A.; Melo, P.; Kim, D. M.; Iedema, P. D. Modeling Crosslinking Polymerization in Batch and Continuous Reactors. *Macromol. React. Eng.* **2013**, *7*, 205−220.
(34) Calvo, I.; Hester, K.; Leiza, J. R.; Asua, J. M. Mathematical Modeling of Carboxylated SB Latexes. *Macromol. React. Eng.* **2013**, DOI: 10.1002/mren.201300168.
(35) Hamzehlou, S.; Reyes, Y.; Leiza, J. R. A New Insight into the Formation of Polymer Networks: A Kinetic Monte Carlo Simulation of the Cross-Linking Polymerization of S/DVB. *Macromolecules* **2013**, *46*, 9064−9073.
(36) Tank, C.; Antonietti, M. Characterization of Water-Soluble Polymers and Aqueous Colloids with Asymmetrical Flow Field-Flow Fractionation. *Macromol. Chem. Phys.* **1996**, *197*, 2943−2959.
(37) Moon, M. H.; Kwon, H.; Parks, I. Stopless Flow Injection in Asymmetrical Flow Field-Flow Fractionation Using a Frit Inlet. *Anal. Chem.* **1997**, *69*, 1436−1440.
(38) Messaud, F. A.; Sanderson, R. D.; Runyon, J. R.; Otte, T.; Pasch, H.; Williams, S. K. An Overview on Field-Flow Fractionation Techniques and their Applications in the Separation and Characterization of Polymers. *Prog. Polym. Sci.* **2009**, *34*, 351−368.
(39) Podzimek, S. *Light Scattering, Size Exclusion Chromatography and Asymmetric Flow Field Flow Fractionation*; John Wiley & Sons: New York, 2011.
(40) do Amaral, M.; Roos, A.; Asua, J. M.; Creton, C. Assessing the Effect of Latex Particle Size and Distribution on the Rheological and Adhesive Properties of Model Waterborne Acrylic Pressure-Sensitive Adhesives Films. *Colloid Interface Sci.* **2005**, *281*, 325−338.
(41) Garret, J.; Lovell, P. A.; Shea, J. A.; Viney, R. D. Water-Borne Pressure-Sensitive Adhesives: Effects of Acrylic Acid and Particle Structure. *Macromol. Symp.* **2006**, *151*, 487−496.
(42) Deplace, F.; Carelli, C.; Langenfeld, A.; Rabjohns, M. A.; Foster, A. B.; Lovell, P. A.; Creton, C. Controlled Sparse and Percolating Cross-Linking in Waterborne Soft Adhesives. *ACS Appl. Mater. Interfaces* **2009**, *1*, 2021−2029.
(43) Deplace, F.; Rabjohns, M. A.; Yamaguchi, T.; Foster, A. B.; Carelli, C.; Lei, C. H.; Ouzineb, K.; Keddie, J. L.; Lovell, P. A.; Creton, C. Deformation and Adhesion of a Periodic Soft−Soft Nanocomposite Designed with Structured Polymer Colloid Particles. *Soft Matter* **2009**, *5*, 1440−1447.
(44) Zosel, A.; Schuler, B. The Influence of Surfactants on the Peel Strength of Water-Based Pressure Sensitive Adhesives. *J. Adhes.* **1999**, *70*, 179−195.
(45) Kinning, D. J. Bulk, Surface, and Interfacial Characterization of Silicone−Polyurea Segmented Copolymers. *J. Adhes.* **2001**, *76*, 1−26.
(46) Paiva, A.; Sheller, N.; Foster, M. D.; Crosby, A. J.; Shull, K. Microindentation and Nanoindentation Studies of Aging in Pressure-Sensitive Adhesives. *Macromolecules* **2001**, *34*, 2269−2276.
(47) Mallégol, J.; Dupont, O.; Keddie, J. L. Morphology and Elasticity of Waterborne Acrylic Pressure-Sensitive Adhesives Investigated with Atomic Force Microscopy. *J. Adhes. Sci. Technol.* **2003**, *17*, 243−259.
(48) Higuchi, W. I.; Misra, J. Physical Degradation of Emulsions via the Molecular Diffusion Route and the Possible Prevention Thereof. *J. Pharm. Sci.* **1962**, *51*, 459−466.
(49) Ugelstad, J.; Mork, P. C.; Mfutakamba, H. R.; Soleimany, E.; Nordhuus, I.; Schmid, R.; Berge, A.; Ellingsen, T.; Aune, O. Thermodynamics of Swelling of Polymer Oligomer and Polymer−Oligomer Particles. Preparation and Application of Monodisperse Polymer Particles. In *Science and Technology of Polymer Colloids*; Poehlein, G. W., Ottewill, R. H., Goodwin, J. W., Eds.; NATO ASI Series E67; Nijhoff: Boston, MA, 1983; pp 51−99.
(50) Daniloska, V.; Tomovska, R.; Asua, J. M. Designing Tubular Reactors to Avoid Clogging in High Solids Miniemulsion Photopolymerization. *Chem. Eng. J.* **2013**, *222*, 136−141.
(51) Benedek, I. *Pressure Sensitive Formulation*; VSP: Utrecht, The Netherlands, 2000.
(52) The Polyurethanes Raw Materials Analysis Committee (PURMAC): Determination of NCO Content of Aromatic Isocyanates. *J. Cell. Plast.* **1991**, *27*, 459−483.
(53) Zosel, A. The Effect of Fibrilation on the Tack of Pressure Sensitive Adhesives. *Int. J. Adhes. Adhes.* **1998**, *18*, 265−271.
(54) Lakrout, H.; Sergot, P.; Creton, C. Direct Observation of Cavitation and Fibrillation in a Probe Tack Experiment on Model Acrylic Pressure-Sensitive-Adhesives. *J. Adhes.* **1999**, *69*, 307−359.
(55) Lakrout, H.; Creton, C.; Ahn, D.; Shull, K. R. Influence of Molecular Features on the Tackiness of Acrylic Polymer Melts. *Macromolecules* **2001**, *34*, 7448−7458.
(56) Deplace, F.; Carelli, C.; Mariot, S.; Retsos, H.; Chateauminois, A.; Ouzineb, K.; Creton, C. Fine Tuning the Adhesive Properties of a Soft Nanostructured Adhesive with Rheological Measurements. *J. Adhes.* **2009**, *85*, 18−54.
(57) Tobing, S. D.; Klein, A. Molecular Parameters and their Relation to the Adhesive Performance of Emulsion Acrylic Pressure-Sensitive Adhesives. II. Effect of Crosslinking. *J. Appl. Polym. Sci.* **2001**, *79*, 2558−2564.
(58) Chauvet, J.; Asua, J. M.; Leiza, J. R. Independent Control of Sol Molar Mass and Gel Content in Acrylate Polymer/Latexes. *Polymer* **2005**, *46*, 9555−9561.
(59) Agirre, A.; Nase, J.; Degrandi, E.; Creton, C.; Asua, J. M. Miniemulsion Polymerization of 2-Ethylhexyl Acrylate. Polymer Architecture Control and Adhesion Properties. *Macromolecules* **2010**, *43*, 8924−8932.
(60) Qie, L.; Dubé, M. A. Influence of Polymer Microstructure on the Performance of Post-Treated Latex-Based Pressure Sensitive Adhesives. *J. Appl. Polym. Sci.* **2012**, *124*, 349−364.